Environmental Toxicology and Pharmacology 94 (2022) 103911

Contents lists available at ScienceDirect

Environmental Toxicology and Pharmacology

journal homepage: www.elsevier.com/locate/etap

Exposure to Polystyrene nanoparticles induces liver damage in rat via induction of oxidative stress and hepatocyte apoptosis

Noha A.E. Yasin [a], Mehrez E. El-Naggar [b,*], Zainab Sabry Othman Ahmed [a,c,**], Mona K. Galal [d], Maha M. Rashad [d], Ahmed M. Youssef [e], Ebtihal M.M. Elleithy [a]

[a] Cytology and Histology Department, Faculty of Veterinary Medicine, Cairo University, Giza, Egypt
[b] Textile Research Division, National Research Centre, Dokki, Cairo, Egypt
[c] Faculty of Veterinary Medicine, King Salman International University, Ras Sudr, South Sinai, Egypt
[d] Biochemistry and Chemistry of Nutrition Department, Faculty of Veterinary Medicine, Cairo University, Giza, Egypt
[e] Packaging and packing materials Department, National Research Center, Dokki, Cairo, Egypt

ARTICLE INFO

Dr. Alan Jeffrey Hargreaves

Keywords:
Polystyrene nanoparticles
Oxidative stress
Apoptosis
Liver
Rats

ABSTRACT

Plastic products are widely used in different applications. Thus, exposure of human and other organisms to these products may affect their biological system. The current study was conducted to investigate the potential deleterious effect of Polysterene nanoparticles (PS-NPs) on the liver and to state the cellular and molecular mechanisms associated with exposure to PS-NPs.30 male rats were divided randomly and equally into 3 groups; control (distilled water), low dose (3 mg/kg/day) and high dose (10 mg/kg/day) exposed group via oral gavage for 5 successive weeks. PS-NPs caused elevation in ALT, AST and MDA, upregulation of apoptosis-related genes and significant decrease in GSH and mRNA expression for antioxidant-related genes (Nrf-2 and GPx). Moreover, alterations in hepatic tissue architecture and positive caspase-3 expression was noticed in a dose- dependent manner. Collectively, PS-NPs can induce hepatoxicity in rats in a dose dependent manner, so the health risk of PS-NPs should not be ignored.

1. Introduction

One of the most widely distributed non-natural products that have pervaded the earth's surface environment is plastic (Zalasiewicz et al., 2016). As known, plastic products have been used daily in many different applications particularly for medical domains (Rhodes, 2018). The nanosized particles [plastic particles of size less than 1 μm (Gigault et al., 2018) are more favorable to be used in various human applications than micro and bulk particles owing to the small size, high surface area and their great activities. Human exposure to micro- and nanoplastic occurs mainly via ingestion as these particles are derived from food packaging (Smith et al., 2018) and plastic water containers (Zuccarello et al., 2019). However, it could also occur via inhalation (Yong et al., 2020). Polystyrene (PS) is one of the most detected plastics in the world (Sen et al., 2018; Gelbke et al., 2019). It is widely used for personal care products, drug delivery, bioimaging, and biosensor when its size reaches microscale or nanoscale (Han et al., 2017; Cooley et al., 2018; Zheng et al., 2019).

The effect of microplastics (MPs) and nanoplastics (NPs) on the mammalian tissues and cells, particularly human, are still not clear (Wright and Kelly, 2017; Rubio et al., 2020). However, some studies have shown the adverse effect of MPs and NPs in mammalian models and reported the accumulation of these particles in the gut, liver, and kidneys (Yang et al., 2019). MP/NP has been documented to exhibit pathological manifestations in fish; including changes in the epithelial barrier integrity, in addition to inflammation and oxidative stress induction (Qiao et al., 2019). Moreover, changes in gut microbiota were also reported (Chen et al., 2018). Regarding its effect on the hepatic tissue, MP/NP was recorded to induce changes in liver metabolites, key metabolic enzymes and oxidative stress induced enzymes (Brun et al., 2019). Rarely, MPs/NPs have been detected in the brain tissue of fish (Ding et al., 2018). In mice, ingested MPs/NPs were found in the gut,

* Corresponding author.
** Corresponding author at: Faculty of Veterinary Medicine, King Salman International University, Ras Sudr, South Sinai, Egypt.
E-mail addresses: nohayassin428@yahoo.com, nohayassin428@cu.edu.eg (N.A.E. Yasin), mehrez_chem@yahoo.com (M.E. El-Naggar), Zainab.sabry@cu.edu.eg (Z.S.O. Ahmed), monagalal12@gmail.com (M.K. Galal), maha_mansour@live.com (M.M. Rashad), Drahmedyoussef1979@gmail.com (A.M. Youssef), eelleithy@hotmail.com (E.M.M. Elleithy).

https://doi.org/10.1016/j.etap.2022.103911
Received 28 October 2021; Received in revised form 4 June 2022; Accepted 14 June 2022
Available online 17 June 2022

kidneys and in the hepatic tissue (Deng et al., 2017; Yang et al., 2019). Intestinal inflammation (Li et al., 2020) and reduction of mucous secretion (Lu et al., 2018) were detected. Moreover, inflammation of the liver, lipid accumulation and changes of lipid profile were also reported (Deng et al., 2017; Luo et al., 2019; Lu et al., 2018). However, a study with mice exposed to PS-MPs in feeding exhibited no detectable lesions or detectable inflammatory response (Stock et al., 2019).

Since PS-NPs are removed from blood stream via the liver, we aimed to study their effect on the hepatic tissue of rats. To our knowledge, this is the first study to investigate the cellular and molecular mechanisms associated with exposure to two different doses of Polystyrene nanoparticles (PS-NPs) in rat hepatic tissue through estimation of the liver function, antioxidant status, and genetic alterations. In addition, histopathological and immunohistochemical changes were evaluated.

2. Material and methods

2.1. Chemicals and reagents

The chemicals that were used in this study include polyvinylpyrrolidone (PVP, Mw = ~29000), styrene monomer (99.9 %) was purchased from Sigma-Aldrich (USA), potassium peroxodisulphate (PPS) were purchased from Merck Co. (Germany). For all experiments, deionized water (Barnsted, Nanopure Ultrapure Water System) was used. Before using styrene for the preparation of nanoparticles, it was distilled under reduced strain. All other chemicals were used exactly as they were provided to us.

2.2. Preparation of polystyrene nano-emulsion

A dispersion polymerization process was used to create polystyrene (PS) microspheres with a mean size of 1.0 μm. In a classic preparation technique, 16 g of styrene monomer, 0.12 g of Polyvinylpyrrolidone (PVP, Mw = ~29000), 20 mL of H_2O and 0.30 g of potassium peroxodisulphate (PPS) as water soluble initiator, were dissolved in 100 mL of ethanol. The achieved solution was then added into a 250 mL three neck round bottom flask with a magnetic stirrer, a refluxing condenser, and a nitrogen inlet. Afterward sealing in a nitrogen atmosphere, the reactor was immersed in water bath and the polymerization process was carried out at 80 °C for 12 h. Then, the acquired polystyrene microspheres were washed by water and redispersed in 50 mL of ethanol. The polystyrene dispersed solution was obtained and placed in an oven at 40 °C for 3 days till the ethanol was totally vaporized. Finally, the uniform polystyrene colloidal crystals were acquired. Then, polystyrene (PS) microspheres were converted to nano-emulsion by dissolving the produced microparticles in a solution of dimethyl sulfoxide (DMSO) with a concentration of 250 mg/100 mL of DMSO and kept under stirring for 60 min. After complete dissolution, Tween 80 (200 mg/50 mL of distilled water was added with continuous stirring for another 60 min. Tween 80 was acted as stabilizing agent. Finally, DMSO solution was removed under evaporating system. The prepared polystyrene nano-emulsion (PS-NPs) was kept in refrigerator for further characterization and application.

2.3. Characterizations

2.3.1. Particle size and zeta potential of the prepared PS nanoparticles

The hydrodynamic particle size for PS-NPs was examined via dynamic light scattering techniques (NICOMP 380 ZLS, Dynamic light scattering (DLS) instrument. PSNPs' zeta potential was measured using a Zetasizer Nano ZS90 (Malvern, Malvern UK). In triplets, separate dispersions of the particles were prepared. From the three results, an average was calculated and given as a result.

2.3.2. Transmission electron microscopy (TEM)

The morphology of the fabricated polystyrene nano-emulsion (PS-NPs) was identified through Transmission electron microscopy (TEM, JOEOL Co., JEM-2100, Tokyo, Japan), under a high-tension electricity of 160 kV at room temperature. The images were taken at appropriate magnifications (low and high magnifications) to estimate the shape and surface of PS-NPs.

2.4. Experimental protocol and animal grouping

2.4.1. Experimental animals and ethical approval

A total number of thirty adult male albino rats (180–200 g) were purchased from the Animal Health Research Institute, Dokki, Egypt. The rats were housed in plastic cages (dimensions 43 cm × 40 cm × 29 cm), five animals were housed in each cage, with stainless steel top grills (netted cover) and soft wood shavings employed as bedding. They were maintained under good hygienic conditions and standard laboratory conditions (controlled atmosphere; standardized temperature, humidity, and light conditions) at a temperature of 22 ± 2 °C, a dark/light cycle of 12 and 50–70 % humidity. Standard food and water were provided ad libitum. The experimental protocol followed NIH guidelines and was accepted by the Faculty of Veterinary Medicine's Institutional Animal Care and Use Committee (IACUC) (Protocol No.: Vet CU28/04/2021/294).

2.4.2. Experimental design and treatment

Following a one-week acclimatization period, rats were divided into three groups at random (n = 10 rats/group). Each group was assigned into 2 cages (n = 5 rats/cage). Control group was served as a negative control (rats received only distilled water). Low dose- treated group received 3 mg/kg/day of PS-NPs, while high dose- treated group received 10 mg/kg/day of PS-NPs according to Amereh et al. (2020). PS-NPs treatments were given with oral gavage, once daily for 5 successive weeks.

2.5. Sample collection and preparation

Blood samples were collected from medial canthus of the eye in clean test tubes, allowed to clot, and then centrifuged for 10 min at 3000 rpm to separate the serum that was kept at −20 °C for determination of liver function markers. After collection of blood samples, rats were euthanized by cervical dislocation, and liver specimens were retrieved from each rat. Some liver samples were preserved at −80 °C for the evaluation of oxidative stress biomarkers and quantitative real-time PCR (qRT-PCR) analysis of certain antioxidant-and apoptotic-related genes. Others were histopathologically and immunohistochemically examined after being fixed in 10 % neutral-buffered formalin solution (10 % NBF).

2.6. Biochemical investigation

2.6.1. Determination of liver function markers

The activities of serum alanine aminotransferase (ALT) and aspartate aminotransferase (AST) were measured using reagent kits (Spectrum Diagnostics Co.) according to the manufacturer's instructions.

2.6.2. Determination of oxidative stress biomarkers

Liver tissue specimens were homogenized in cold phosphate buffer saline then the tissue homogenates were used to determine reduced glutathione (GSH) according to Ellman (1959) and lipid peroxidation biomarker; malondialdehyde (MDA) according to Ohkawa et al. (1979), in addition to total protein concentration as described by Bradford (1976).

2.6.3. qRT-PCR analysis for Nrf-2, GP_X, Cytc, and CASP 3

The relative hepatic Nrf-2, GPX, Cytc, and CASP 3 mRNA abundance was determined by qRT-PCR analysis using GAPDH as a housekeeping gene. Total RNA was extracted from approximately 100 mg of hepatic tissue using total RNA Extraction Kit (Vivantis, Malaysia). RT-PCR was

performed using M-MuLV Reverse Transcriptase (NEB#M0253) after confirming the concentration and purity of RNA. Quantitative assessment of cDNA amplification for each gene was performed by a fluorescence-based real-time detection method with a fluorescent SYBR Green dye (Thermo Scientific, Cat. No. K0221). The primer pairs of Nrf 2 gene (Accession number, NM_031789.3) sense primer: 5′-TGTCAGCTACTCCCAGGTTG-3′; antisense primer: 5′-ATCAGGGGTGGTGAAGACTG-3′, GPX gene (Accession number, M21210.1) sense primer: 5′-GGCCCTCAATAGTGCTCAG-3′ antisense primer 5′-CCACCACCGGGTCGGACATAC-3′ **Cytc** gene (Accession number, NM_012839.2) sense primer: 5′- GGCAAGCATAAGACTGG ACC−3′ antisense primers: 5′- GTCTGCCCTTTCTCCCTTCT−3′, CASP 3 gene (Accession number, NM_012922.2) sense primer: 5′-GGAGCTTGGAACGCGAAGAA-3′ antisense primer: 5′-ACACAAGCCCATTTCA GGGT-3′, and GAPDH gene (Accession number, NM_017008.4) sense primer: 5′-ACCACAGTCCATGCCATCAC-3′ antisense primer: 5′-TCCACCACCCTGTTGCTGTA-3′. The real-time PCR conditions were performed as follows: 95 ^{o}C for 5 min (initial denaturation) and then 40 cycles at 95 ^{o}C for 15 s, 60 ^{o}C for 30 s, and 72 ^{o}C for 30 s. In each experiment, negative controls that were free of the template were included. Each qRT-PCR was performed with three biological replicates and each biological replicate was assessed three times. The relative transcription levels were calculated using the comparative 2−ΔΔCT method (Livak and Schmittgen, 2001).

2.7. Histopathological examination

2.7.1. Light microscopy

Liver samples, from all groups, were carefully dissected out, fixed in 10 % NBF for 48 h, washed, embedded in ascending grades of ethanol for tissue dehydration, then the tissue sections were cleared in xylene, embedded in paraffin wax, sectioned at 3–4 μm thickness, deparaffinized, and eventually stained with hematoxylin and eosin (H&E) stain (Bancroft and Gamble, 2008).

Microscopic grading and scoring of the pathological lesions of the hepatic sections were assessed in five rats per group. According to the dissemination and severity of histopathological alterations, the noticed pathological lesions were scored as (−): normal histology, (+): mild (less than 25 %), (++): moderate (from 25 % to 50 %), (+++): severe (from 51 % to 75 %), and (++++): very severe (more than 75 %) (Michael, 2008).

2.7.2. Immunohistochemical examination for Caspase 3

4 μm thick deparaffinized hepatic sections were prepared for the caspase 3 immunohistochemical examination for detection of apoptosis according to manufacturer's protocol. Deparaffinized sections were treated with H_2O_2 at concentration 0.3 % in phosphate-buffered saline (PBS) for 20 min in order to block the activity of endogenous peroxidase, then it was followed by incubation with Mouse anti-active caspase 3 antibody (bsm33199M- Sun Long Biotech Co., LTD) 1:100 for 1 hr, then they were washed out by PBS and incubated with secondary antibody Horse Radish peroxidase (HRP) Envision Kit (DAKO) for 20 min, washed out and incubated with diaminobenzidine (DAB) for 15 min. Then, tissue sections were washed by PBS, counterstained with hematoxylin, dehydrated, cleared in xylene, and covered with the coverslip for microscopic examination.

2.7.3. Evaluation of immunohistochemical observations (Area %)

Caspase-3 was used for evaluation of apoptosis in liver tissue. Avidin-biotin- peroxidase technique was used for detection of activated caspase-3 according to Hsu et al. (1981). Immunohistochemically stained liver sections were analyzed using Leica Quin 500 software for morphological analysis (Leica Microsystems, Switzerland). The image analyzer was caliberated automatically to convert the measurement units (pixels) produced by image analyzer program into actual micrometer units. Immunohistochemical reactions were measured as area percent in a standard 5 microscopic fields from different sections in each group using magnification (X400) by light microscopy transferred to the monitor's screen. Regardless of the severity of the staining, the areas displaying positive caspase 3 immunostaining (brown color) were chosen for estimation. Each specimen's mean value and standard error mean (SEM) were calculated and statistically analyzed.

2.8. Statistical analysis

The data was analyzed using one-way analysis of variance (ANOVA) by SPSS version 17.0 software (IBM, USA) to assess the significance of the mean between the groups, followed by an LSD post hoc test. Statistical significance was described as a *P*-value less than 0.05.

3. Results

3.1. Characterization of PS-NPs

As observed from Fig. 1A and B that, the resultant PS-NPs were examined using TEM at different magnifications to illustrate their particle shape. The PS-NPs are found to have a perfect spherical morphology with an average diameter of about 25 nm. Furthermore, TEM images demonstrate that PS-NPs do not form particle aggregates or agglomerates but formed with monodispersed particles.

DLS was also used to determine the average hydrodynamic size of the synthesized PS-NPs, revealing that they have an average size of 92 nm and a polydispersity index (PDI) of 0.394 Fig. 2A. Thus, due to the obtained particle small size with small size and low polydispersity index (Honary et al., 2012), PS-NPs are single particles that can have a positive impact on biological domains, as shown in Fig. 2A. The disparity between DLS and TEM average sizes is since DLS emphasizes the hydrated diameter combined with the water coating layer, while TEM does not.

In addition, the surface charge furthermore controls the dispersion or agglomeration of the particles, which directly determine the bioavailability of PS-NPs. PS-NP aggregation would result in larger particle sizes (micrometres), which would reduce PS-NP absorption and acute toxicity. Fig. 2B shows the values of zeta potential of PSNPs (−30.6 mv) indicating that the PS-NPs prepared with high stability. Overall, PS-NPs appeared to have spherical shape with high stability.

3.2. Biochemical investigation

3.2.1. Effect of PS-NPs on liver function

Hepatic damage was estimated by determination of ALT and AST activities. According to the obtained data in Fig. 3A and B, the low dose-treated group revealed a significant increase in ALT activity from 41.31 U/L to 47.42 U/L and AST activity from 96.7 U/L to 142.67 U/L when compared to the control group. Similarly, the high dose-treated group also revealed a substantial increase in ALT and AST activities to 65.47 U/L and 153.37 U/L respectively compared to the control group. Furthermore, as opposed to the low dose-treated group, the high dose-treated group exhibited a remarkable increase (p<0.05) in ALT activity and a non-remarkable increase (p< 0.05) in AST activity.

3.2.2. Effect of PS-NPs on the cellular redox state

For studying the redox state of the cell, oxidative stress biomarkers (MDA, and GSH), some antioxidant related gnes (Nrf-2 and GPx) were estimated.

3.2.2.1. Oxidative stress biomarkers

3.2.2.1.1. MDA content in the liver. Compared to the control group, the low dose-treated group significantly elevated MDA hepatic content from 1.81 to 2.45 μMmg^{-1} protein, as shown in Fig. 3C. Also, the high dose-treated group significantly increased MDA content to 2.82 μM mg^{-1} protein compared to control. Besides, a substantial elevation (p<0.05) in

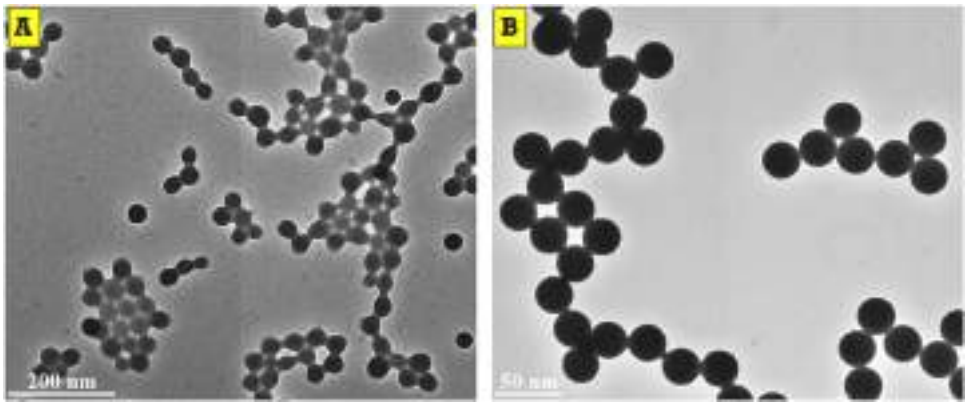

Fig. 1. TEM of PSNPs at (A) low magnification and (B) high magnification.

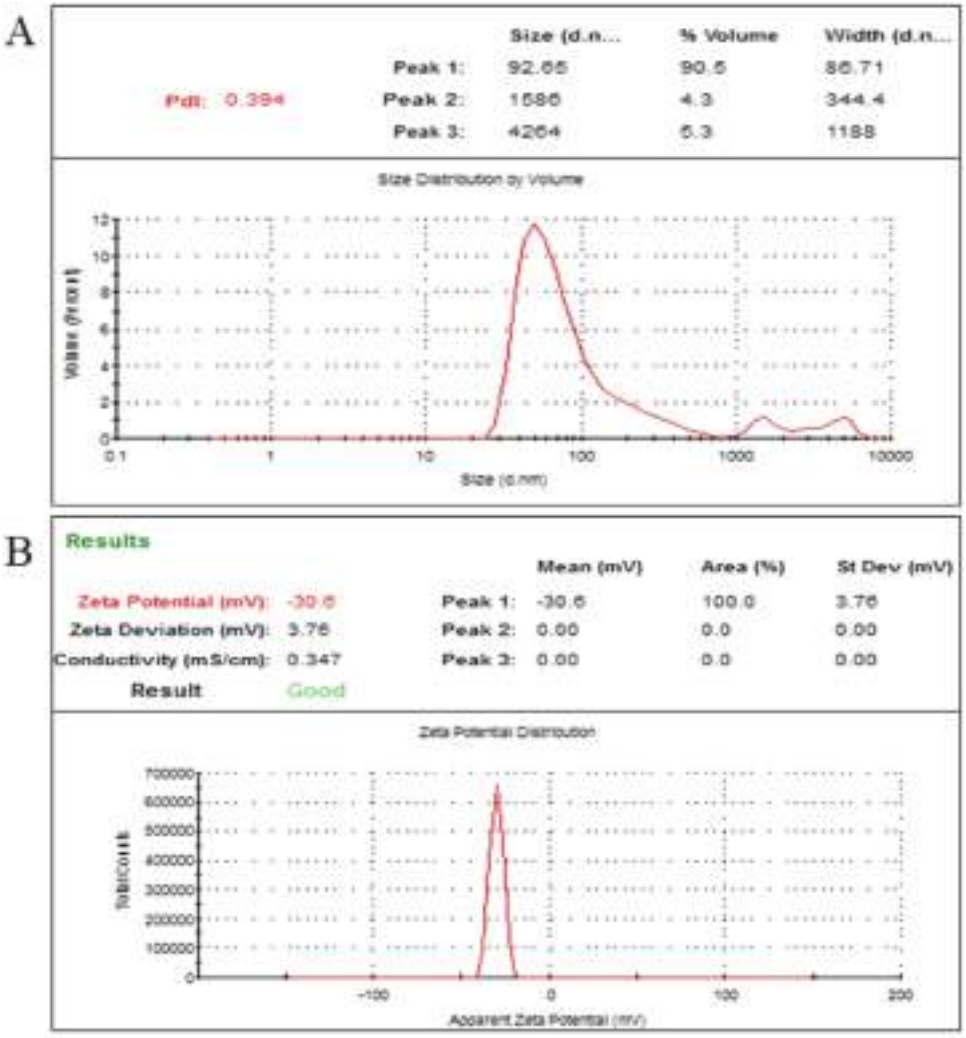

Fig. 2. (A) Hydrodynamic particle size of PSNPs, (B) Zeta potential measurement of PSNPs.

MDA activity was observed in the high dose- treated group when compared with the low dose- treated group.

3.2.2.1.2. Hepatic GSH content. Compared to the control group, hepatic GSH content was significantly reduced from 3.83 to 2.52 and 1.93 μM mg^{-1} protein in male albino rats in both low and high doses-treated groups, respectively. Furthermore, the high dose- treated group exhibited a marked decrease (p<0.05) compared to the low dose- treated group as shown in Fig. 3D.

3.2.2.2. Effect of PS-NPs on hepatic mRNA relative expression for some antioxidant related genes (Nrf-2 and GPx). PS-NPs significantly decreased mRNA expression for Nrf-2–0.84-fold and 0.29-fold in both low and high doses-treated groups, respectively. Also, a significant decline (p<0.05) was noticed in the high dose-treated group when

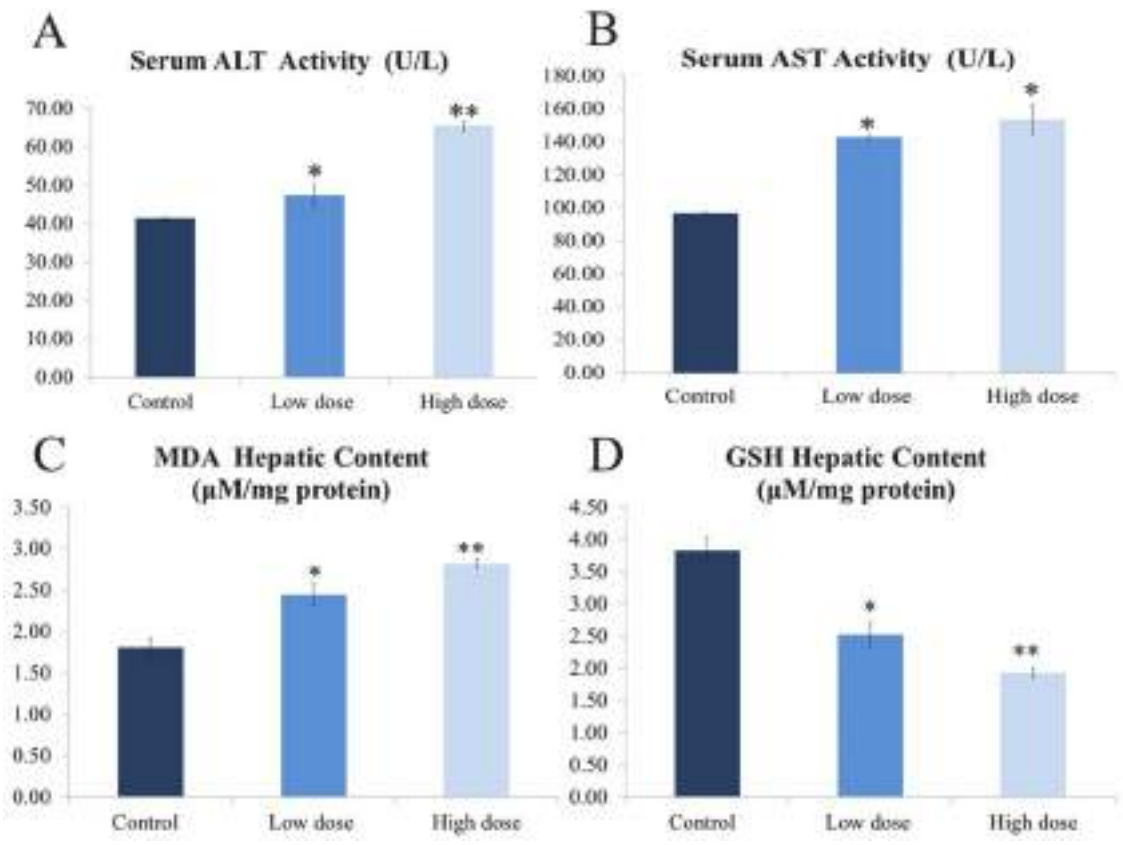

Fig. 3. Effect of PS-NPs on the liver function ((A) ALT (U/L) and (B) AST (U/L)), MDA (µM mg-1 protein) (C) and GSH (µM mg-1 protein) (D) liver content in male albino rats. Data are represented as mean ± SEM. * indicates a significant difference from the comparable negative control at $p<0.05$. **Indicates significant difference from the comparable low dose-treated group at $p<0.05$.

compared to the low dose-treated group as shown in Fig. 4A. Similarly, the low and high doses-treated groups revealed a remarkable decrease in mRNA expression for GPx to 0.93 and 0.20 -fold, respectively, compared to the control group. In addition, there was a significant decline ($p<0.05$) between the low and the high dose- treated group as shown in Fig. 4B.

3.2.3. Effect of PS-NPs on hepatic mRNA relative expression for some apoptotic-related genes (Cytc and CASP 3)

Our current data revealed that both low and high doses-treated groups resulted in a noticeable increase in mRNA expression for **Cytc** to 6.45-fold and 7.30-fold, respectively, compared to the control group. Also, CASP 3 gene expression was significantly elevated to 2.42-fold and 6.45-fold in both low and high doses-treated groups, respectively, when compared to the control group. Moreover, in comparison to the low dose-treated group, the high dose- treated group revealed a significant upregulation ($p< 0.05$) in mRNA expression for both **Cytc** and CASP 3 as shown in Fig. 4C and D.

3.3. Histopathological and immunohistochemical investigations

3.3.1. Effect of PS-NPs on liver by light microscopy

Examination of H&E-stained liver sections of rats from the control group exhibited normal, intact, homogenous hepatic parenchyma with regular hepatic cords that were radiating from a normal central vein and separated by normal hepatic sinusoids (Fig. 5A). Polygonal hepatocytes with large, vesicular, spherical nuclei and prominent nucleoli were observed (Fig. 5A and B). Furthermore, a normal portal triad containing the bile duct, portal vein, and hepatic artery emerged between hepatic lobules (Fig. 5C).

On the other hand, liver sections of PS-NPs-exposed rats demonstrated variable hepatic damage varied in severity according to the administrated dose. Liver sections from the low dose- treated group revealed obvious dilatation and moderate congestion of the central vein (Fig. 5D), in addition to dilatation and congestion of the hepatic sinusoids with Kupffer cell activation and pyknosis (Fig. 5E). Moderate disorganization of hepatic parenchyma was also plentiful (Fig. 5E). Moreover, hepatocellular degeneration was detected in the form of moderate hydropic degeneration as some hepatocytes displayed ballooning with mild to moderate cytoplasmic vacuolization, in addition to nuclear condensation (Fig. 5F). Also, abnormal mitosis was noticed (Fig. 5G). PS-NPs deposition (dark brown coloration) was also detected in some hepatocytes (Fig. 5H). Additionally, the portal triad was observed with a congested portal vein, shrunken bile duct, and mild inflammatory cell infiltration (Fig. 5I).

However, liver sections from the high dose- treated group exhibited central vein with severe dilatation, and blood engorgement (Fig. 6A). Also, blood sinusoids were severely dilated and engorged with blood and edema. Kupffer cells' activation, proliferation, and pyknosis were noticeable. Furthermore, hepatic cords were severely disrupted (Fig. 6B). Severe hydropic degeneration of the hepatocytes with marked diffuse cytoplasmic vacuolization and apoptosis were observed (Fig. 6C). Abnormal mitosis (Fig. 6B) and mitotic figures (Fig. 6C) were also evident. Additionally, karyolysis was pronounced (Fig. 6D and E). Most hepatocytes showed PS-NPs deposition as well as irregularity and disruption of the central vein's wall (Fig. 6E). Moreover, the portal triad was enlarged by moderate inflammatory cellular infiltration and appeared with the congested portal vein and deteriorated bile duct (Fig. 6F).

The results of the hepatic microscopic lesions grading were summarized in Table 1.

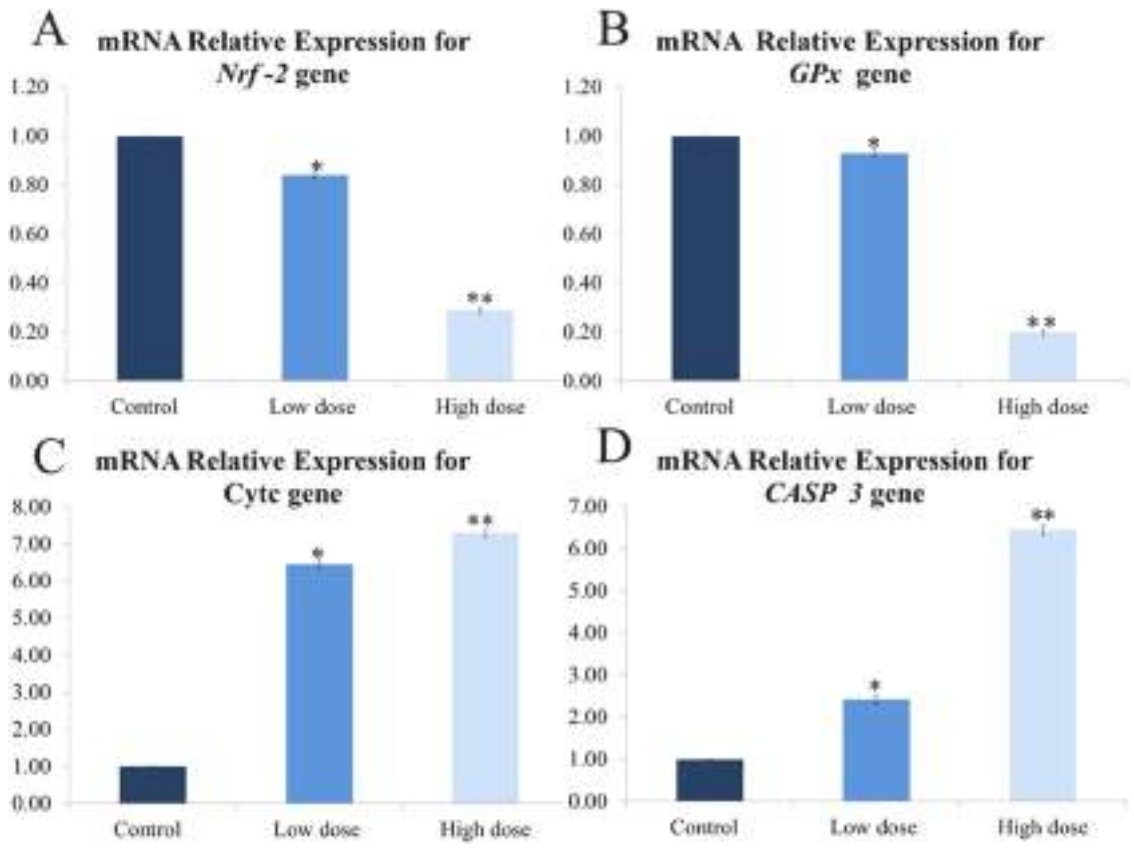

Fig. 4. Effect of PS-NPs on liver mRNA relative expression for Nrf-2 (A), GPx (B), Cytc (C), and CASP3 (D) in male albino rats. Data are represented as mean ± SEM. * indicates significant difference from the corresponding control negative group at $p<0.05$. **Indicates significant difference from corresponding low dose-treated group at $p<0.05$.

3.3.2. Effect of PS-NPs on caspase-3 immunohistochemistry

Compared to the untreated control group, the low dose-treated group exhibited a moderate immunoreactivity for caspase-3 (Fig. 7B) with a significant increase in the area % from 7.74 to 16.16 (Fig. 7), while the high dose-treated group showed a strong immunoreactivity (Fig. 7C) with a substantial increase in the area % to 38.04 (Fig. 7). Besides, the high dose- treated group revealed a significant elevation ($p<0.05$) in the area % compared to the low dose- treated group as shown in Fig. 7.

4. Discussion

The extensive use of plastics has posed serious problems to the environment, human and animal health as well. One of the extensively used plastic nanoparticles is PS-NPs. The toxicity and the mechanism of toxicity induced by PS-NPs in the animal model are not fully understood (Hu and Palić, 2020). To our knowledge, this is the first study to investigate the cellular and molecular mechanisms associated with exposure to two different doses of Polystyrene nanoparticles (PS-NPs) in rat hepatic tissue. Numerous technological and biomedical implementations have been occurred for nanoparticles of various shapes, sizes, and structures (Soenen et al., 2015; Amiri et al., 2019). Nanoparticles have characteristics that differ from bulk materials because of their high surface to volume ratio. Polystyrene particles acted less cytotoxic on non-phagocytic cells (Ref; Cellular Targets and Mechanisms in the cytotoxic action of non-biodegradable Engineered Nanoparticles. The cytotoxicity results of the work designed by Jangsun Hwang et al. (reference: Potential toxicity of polystyrene microplastic particles) showed that PS particle concentrations of 500 g/mL did not impair the viability of HDF cells and PBMCs. A high concentration (1000 g/mL) however, induced cytotoxicity in up to 50 % of HDF cells. Thus, in our current work, polystyrene nano-emulsion (PS-NPs) was easily synthesized using Tween 80 as both emulsifier and stabilizing agent that can protect the particles of PS-NPs from agglomeration. In the current study, we used different two exposure doses of PS-NPs to reduce the knowledge gap regarding the PS-NPs hepatic dysfunction and to provide new insights on the possible mechanism for its toxicity in the rat models. The liver has a vital role in the removal of nanoparticles from the bloodstream through converting these xenobiotics into more water-soluble compounds by its transforming enzymes (Bouteraa et al., 2020). AST and ALT are two of the most critical parameters to consider when assessing NPs hepatic toxicity. As a result, elevated levels of ALT and AST can be a sign of hepatocyte destruction, either as a result of NPs' direct toxic effects or as a result of the immune system's response (Bouteraa et al., 2020). In the current research, we discovered that oral administration of PS-NPs induces a substantial ($p<0.05$) elevation in serum AST and ALT function in a dose-dependent manner, which is indicative of liver damage. Since these enzymes are primarily located in the cytoplasm of hepatic cells, their excretion into the blood may be due to cell injury. These results are concordant with those reported by Amereh et al. (2019). These PS-NPs induced liver damage that was manifested histopathologically by alteration in the normal histological architecture of the hepatic tissue that varied in severity depending on the administrated dose. These histopathological findings are consistent with Lu et al. (2018) and Luo et al. (2019). The induced hepatic dysfunction may be a consequence of gut toxicity that resulted in impairment of the gut vascular barrier that, in turn, might lead to or that, in turn, lead to the entrance of PS-NPs into the circulation and allow these particles to gain access to the hepatic tissue through the portal vein, as suggested by Deng et al. (2018) and Yang et al. (2019). The bioaccumulation of PS-NPs particles in the hepatic tissue was noticed in the present study as brown-colored deposition in hepatocytes (Figs. 5g and 6 e). This result is supported by Deng et al. (2017) and Pitt

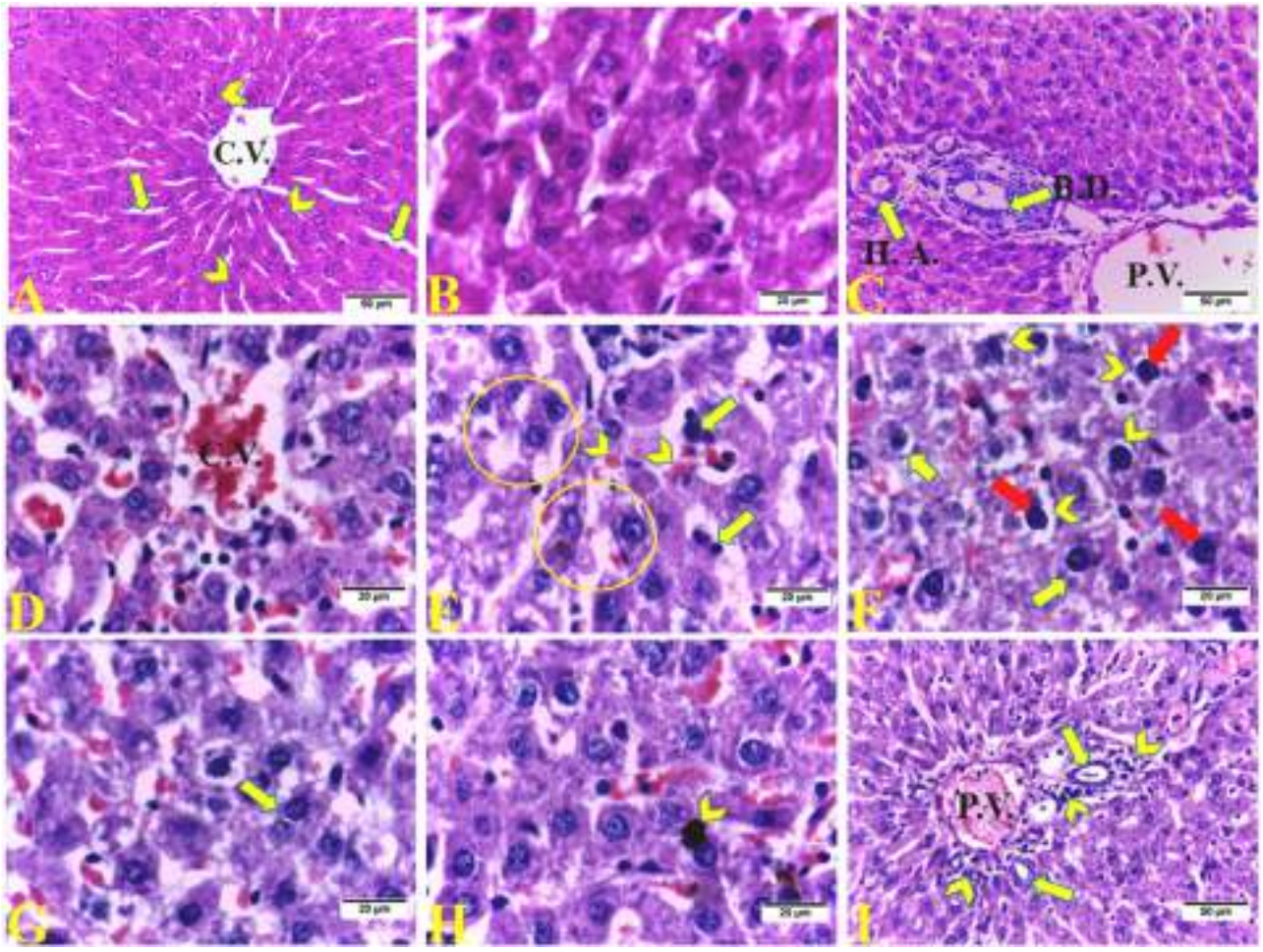

Fig. 5. (A:C) Liver sections from control male albino rats showing (A) Hepatocytes (chevron) radiating from central vein (C.V.) in the form of cords with large, vesicular, and spherical nuclei and separated by normal hepatic sinusoids (yellow arrows) (H&E, X400). (B) High magnification of control hepatocytes (H&E, X1000). (C) Portal triad appears with normal bile duct (B.D.) lined by cuboidal epithelium (yellow arrow), portal vein (P.V.) and hepatic artery (H.A.) (H&E, X400) (D:I) Liver sections from low dose-treated group revealing (D) Obvious dilatation and moderate congestion of central vein (C.V.) (H&E, X1000) (E) Dilatation and congestion of hepatic sinusoids (chevron) with Kupffer cell activation and pyknosis (yellow arrow). Moderate disorganization of hepatic parenchyma is also plentiful (yellow circle). (H&E, X1000) (F) Moderate hydropic degeneration; swelling and ballooning of hepatocytes with mild (yellow arrow) to moderate (chevron) cytoplasmic vacuolization in addition to, nuclear condensation (red arrow) (H&E, X1000) (G) Abnormal mitosis is also observed (yellow arrow) (H&E, X1000) (H) PS-NPs deposition (brown coloration) is also noticed in some hepatocytes (chevron). (H&E, X1000) (I) The portal triad is observed with congested portal vein (P.V.), shrunken bile duct (yellow arrow) and mild inflammatory cell infiltration (chevron) (H&E, X400).

et al. (2018) who observed the accumulation of PS MPs/ NPs in the hepatic tissue of mice and fish, respectively. The criterion for the degree of cellular damage suggests that excess PS-NPs can accumulate in hepatocytes and consequently activate the vacuolation process as the amount of PS-NPs increases, the volume of vacuoles enlarges. The cytoplasmic vacuolization and ballooning degeneration of the hepatocytes may occur due to disturbances of cellular membrane function therefore disruption of fluid and ion homeostasis and the massive influx of Na^{+} and water (Schrand et al., 2010). Another possible explanation of ballooning degeneration could be lysosomal hydrolytic enzymes leakage that can lead to cytoplasmic degeneration of hepatocytes (Del Monte, 2005). In the present study, vascular dilatation and congestion were almost constant features in all the PS-NPs treated groups. Oligny and Lough (1992) have previously explained sinusoidal dilatation on basis of hepatocellular degeneration and necrosis or due to damage of the sinusoidal endothelial cells. Since the Kupffer cell is the primary target for toxicants (Roberts et al., 2007), its activation, proliferation, and pyknosis might be a kind of defense mechanism against PS-NPs -induced hepatic oxidative stress (Neyrinck, 2004). Besides, the inflammatory cell infiltration induced by PS-NPs, we suggest that PS-NPs might interact with the interstitial tissues leading to several immune responses.

ROS induced by NPs is considered as the most suggested mechanism of their toxicity. The induced ROS has been ascribed to the existence of prooxidant groups on their reactive surface or nanoparticle-cell interactions (Yu et al., 2020). In our study, the dose-dependent increases of hepatic MDA level along with the inhibition of GSH content, Nrf-2, and GPx mRNA expression levels were accepted as signs of oxidative stress. MDA is a reliable indicator for oxidative stress. Based on our data, the elevated amounts of MDA and reduced levels of antioxidant parameters point to the enhanced formation of lipid peroxidation resulting in hepatic dysfunction, as well as a deficiency of antioxidant defense against the development of excessive free radicals (Motaghinejad et al., 2015). Moreover, the overproduction of ROS exceeded the ability of cellular antioxidant machinery, resulting in the accumulation of pro-oxidants that led to oxidative stress (Bugata et al., 2019). Free radicals generated by lipid peroxidation led to leakage of liver enzymes as well as damage to biomolecules such as lipids, proteins, and DNA (Faddah et al., 2013). Our findings are in harmony with the recent studies emphasizing that oxidative stress is a potential mechanism involved in PS-NP toxicity (Hazeem et al., 2020; Hu et al., 2021; Ahmed et al., 2022). Nrf2 is a master regulator of the antioxidant battery and detoxification genes with cytoprotective function. It induces the

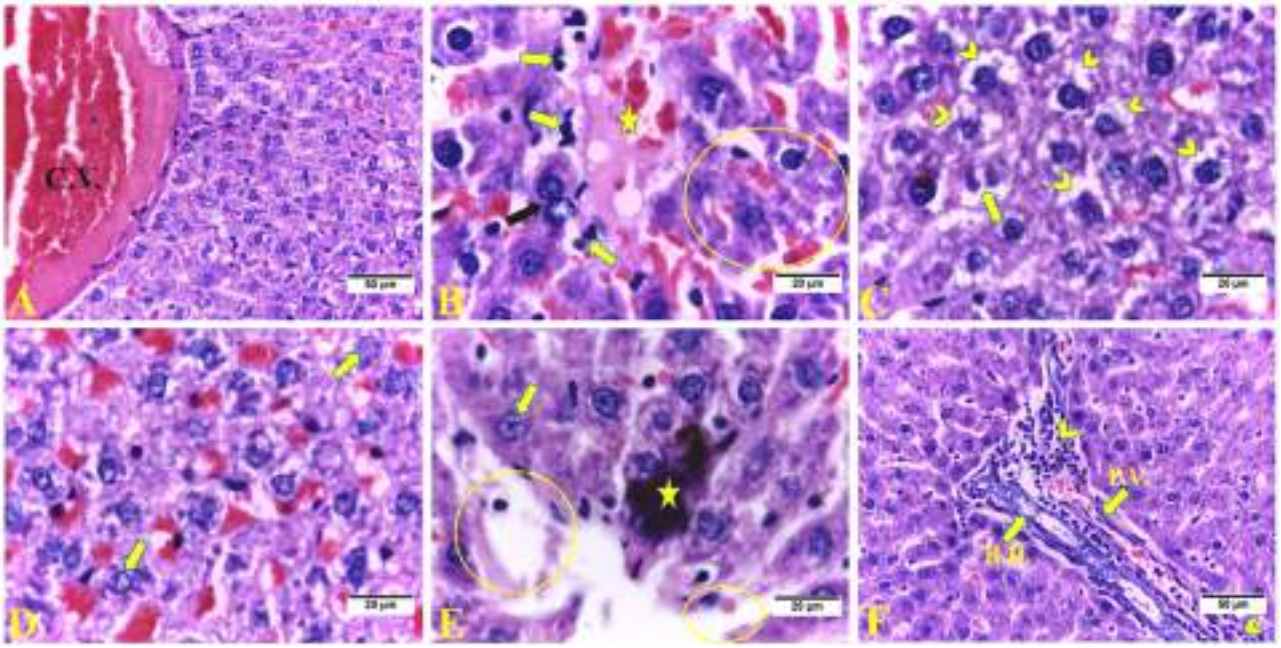

Fig. 6. Liver sections from high dose-treated group demonstrating (A) Central vein (C.V.) with severe dilatation and blood engorgement (H&E, X400). (B) Blood sinusoids are severely dilated and engorged with blood and edema (star) in addition to, Kupffer cells' activation, proliferation and pyknosis (yellow arrow). Hepatic cords are severely disrupted (yellow circle). Also, abnormal mitosis is noticed (black arrow) (H&E, X1000) (C) Severe hydropic degeneration of the hepatocytes with marked diffuse cytoplasmic vacuolization and apoptosis are noticed (chevron). Mitotic figure (yellow arrow) is also evident. (H&E, X1000) (D) Karyolysis is pronounced (yellow arrow) (H&E, X1000) (E) PS-NPs deposition in most hepatocytes (star) and irregularity and disruption of central vein's wall (yellow circle). Also, karyolysis is noticed (yellow arrow) (H&E, X1000) (F) Expanded portal triad by moderate inflammatory cellular infiltration (chevron) and appear with congested portal vein (P.V.) and deteriorated bile duct (B.D.) (H&E, X400).

Table 1
Scoring of histopathological findings observed in the liver sections of different experimental groups.

Items/ groups	Control group	Low dose-treated group	High dose-treated group
Dilatation and Congestion:	–	++	++ +
1. Central Vein		++	++ +
2. Blood Sinusoids		++	++
3. Portal Vein			
Hydropic Degeneration (ballooning and cytoplasmic vacuolization)	–	++	++ +
Deposits	–	+	++
Nuclear Changes:	–	++	++ +
1. Pyknosis			
Portal Area:	–	+	++
1. Inflammatory cell infiltration			

Notes: (-) none, (+) mild, (++) moderate and (+++) severe tissue damage. n = 3 rats/ group.

expression of its target genes by binding to the antioxidant response element (ARE) (Tonelli et al., 2018; Hashim et al., 2022). Inactivation of Nrf2 also is necessary for the complete execution of apoptosis in the presence of extensive cellular damage caused by oxidative stress (Méndez-García et al., 2019). To investigate the oxidative stress mechanism of PS-NPs at the molecular level, the effects of PS-NPs on GPx and Nrf-2 expressions were noticed by real-time PCR. Our findings revealed that the Nrf-2 and GPx mRNA expressions were significantly reduced in PS-NPs-exposed groups in a dose-dependent manner in comparison with those of control group. According to these findings, PS-NPs revealed oxidant effects by activating the Nrf-2 signaling pathway. The antioxidant response component in the promoters of many antioxidant genes, such as GPx and glutathione S-transferases, is binded and activated by Nrf-2 (Xue et al., 2020). Therefore, Nrf-2 controls the antioxidant protective cellular response (Tomasi and Ramani, 2018). Decreased expression of downstream genes in the Nrf-2 pathway and repression of the Nrf2-dependent antioxidant system result from Nrf-2 degradation or suppression of its translocation into the nucleus (Sun et al., 2015). The ability of PS-NPs to produce an inordinate amount of ROS and free radicals was the primary cause of tissue damage (Manke et al., 2013). In addition, inflammation and mitochondrial dysfunction can be induced by the redox imbalance that, in turn, lead to apoptosis. Also, our results revealed that expression of the caspase-3 (proapoptotic protein) and transcription factor Cytc gene was markedly increased in the hepatic tissues of PS-NPs treated rats. Cytc is a transcription factor that regulates cell proliferation, differentiation, and apoptosis. It can stimulate apoptosis when it is over-expressed (Rashad et al., 2018). The activation of Cytc has been suggested to cause processing/activation of caspases (caspase 3) (Hotti et al., 2000). Extrinsic stimuli or intrinsic factors that cause mitochondrial stress may activate caspase-3 in apoptotic cells. Overexpression of both genes in a dose-dependent manner in PS-NPs treated groups may be because of the overproduction of ROS, which caused a substantial increase in caspase-3 activity, resulting in cell death (Zhao et al., 2003). In the current study, the overexpression of caspase-3 was also investigated by immunohistochemical analysis that revealed strong expression in a dose dependent manner in PSNPs -treated groups (Fig. 7). According to Ibrahim et al. (2015), mitochondrial damage can be induced by NPs after endocytotic uptake via the direct interaction with undissolved nanoparticles and/or ROS-derived lipid peroxides resulting in membrane disruption and release of apoptotic enzymes (Semisch et al., 2014). Thus, leading to progressive destruction of hepatocytes in addition to stellate cells activation which plays a vital role in liver injury (Ibrahim et al., 2015). Here, we observed that overproduction of ROS induced by PS-NPs caused mitochondrial damage which, in turn, leading to mitochondrial transmembrane potential loss, subsequent release of cytochrome-C, and cleavage of caspase-3.

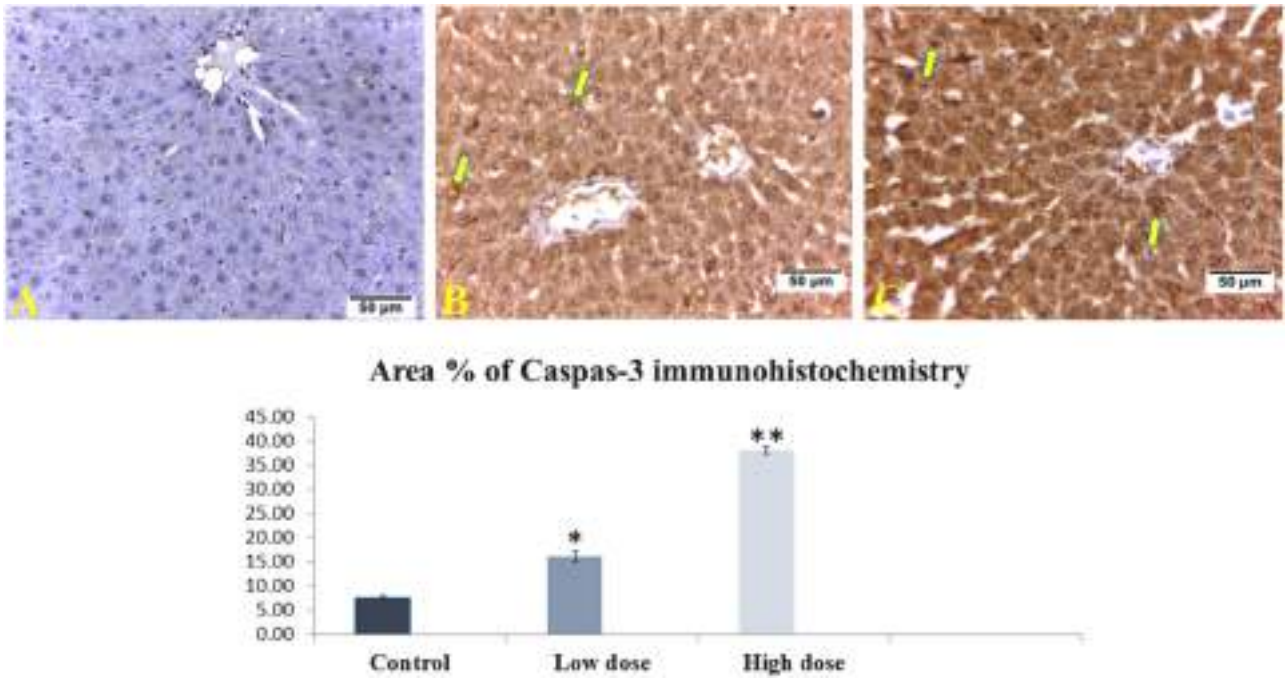

Fig. 7. Effect of PS-NPs on immune expression of caspase-3 in the hepatic tissue sections of different groups (X400) (A) Control rats (B) Low dose-treated group (C) High dose-treated group. Notice, the positive brown immune expression (arrow). Data are represented as mean ± SEM. * indicates significant difference in the area % from the comparable negative control at $p < 0.05$. **Indicates significant difference from the comparable negative control group at $p < 0.05$.

5. Conclusion

Oral administration of PS-NPs at two different doses (3 and 10 mg/kg) daily for 5 successive weeks can induce hepatotoxicity in adult rats in a dose dependent manner. This toxicity was observed through substantial increase in ALT and AST activities, alteration of the histoarchitecture of the hepatic tissue, severe congestion in the central vein and hepatic sinusoids, in addition to hepatocytes degeneration. Moreover, administration of PS-NPs resulted in elevation of MDA concentrations and reduction of GSH levels as well as mRNA relative expression for some antioxidant-related genes (Nrf-2 and GPx), that induced oxidative stress. In addition, overexpression of apoptosis-related genes as **Cytc**, and CASP 3 was also noticed. These findings indicate that oxidative stress is a key risk factor in PS-NPs-induced liver cell death.

Funding

No funds, grants, or other support was received.

Ethics approval and consent to participate

All animals were treated humanely in accordance with NIH guidelines, and the experimental procedure was approved by the Faculty of Veterinary Medicine's Institutional Animal Care and Use Committee (IACUC), Faculty of Veterinary Medicine, Cairo University (Protocol No.: Vet CU28/04/2021/294).

Consent for publication

Not applicable.

Data availability

Not applicable.

CRediT authorship contribution statement

All authors conceived the study and designed the experimental protocol, Mehrez E. El-Naggar and Ahmed M. Youssef prepared polystyrene nanoparticles (PS-NPs) and examined their morphology, Noha A.E. Yasin, Zainab Sabry Othman Ahmed and Ebtihal M. M. Elleithy carried out the histopathological analysis and draft the manuscript, Mona K. Galal and Maha M. Rashad carried out the biochemical analysis, All authors read, revised, and approved the final manuscript.

Declaration of Competing Interest

The authors declare that they have no known competing financial interests or personal relationships that could have appeared to influence the work reported in this paper.

References

Ahmed, Y.H., El-Naggar, M.E., Rashad, M.M., Youssef, A., Galal, M.K., Bashir, D.W., 2022. Screening for polystyrene nanoparticle toxicity on kidneys of adult male albino rats using histopathological, biochemical, and molecular examination results. Cell Tissue Res. 1–17.

Amereh, F., Eslami, A., Fazelipour, S., RafieeM, Zibaiid, M.I., Babaei, M., 2019. Thyroid endocrine status and biochemical stress responses in adult male Wistar rats chronically exposed to pristine polystyrene nanoplastics. Toxicol. Res. 8, 953–963.

Amereh, F., Babaei, M., Eslami, A., Fazelipour, S., Rafiee, M., 2020. The emerging risk of exposure to nano(micro)plastics on endocrine disturbance and reproductive toxicity: from a hypothetical scenario to a global public health challenge. Environ. Pollut. 216, 114158.

Amiri, M., Salavati-Niasari, M., Akbari, A., 2019. Magnetic nanocarriers: evolution of spinel ferrites for medical applications. Adv. Colloid Interface Sci. 265, 29–44.

Bancroft, J.D., Gamble, M., 2008. Theory and Practice of Histological Techniques, 6th ed.,. Churchill Livingstone/Elsevier, Philadelphia, PA.

Bouteraa, Z., Rouabhi, R., Menaceur, F., Gasmi, S., 2020. Cellular apoptosis, mitochondrial swelling, permeability and Cytochrome-c level after (Fe_3O_4)-NPs nanoparticles exposure and protective role of diferuloylmethane in Rat's liver. ASN 7, 140–154.

Bradford, M.M., 1976. A rapid and sensitive method for the quantitation of microgram quantities of protein utilizing the principle of protein-dye binding. Anal. Biochem 72, 248–254.

Brun, N.R., Van Hage, P., Hunting, E.R., Haramis, A.P.G., Vink, S.C., Vijver, M.G., Schaaf, M.J., Tudorache, C., 2019. Polystyrene nanoplastics disrupt glucose

metabolism and cortisol levels with a possible link to behavioural changes in larval zebrafish. Commun. Biol. 2 (1), 1–9.
Bugata, L.S.P., Pitta Venkata, P., Gundu, A.R., Mohammed Fazlur, R., Reddy, U.A., Kumar, J.M., Mekala, V.R., Bojja, S., Mahboob, M., 2019. Acute and subacute oral toxicity of copper oxide nanoparticles in female albino Wistar rats. J. Appl. Toxicol. 39, 702–716.
Chen, L., Hu, C., Lai, N.L.S., Zhang, W., Hua, J., Lam, P.K., Lam, J.C., Zhou, B., 2018. Acute exposure to PBDEs at an environmentally realistic concentration causes abrupt changes in the gut microbiota and host health of zebrafish. Environ. Pollut. 240, 17–26.
Cooley, M., Sarode, A., Hoore, M., Fedosov, D.A., Mitragotri, S., Gupta, A.S., 2018. Influence of particle size and shape on their margination and wall-adhesion: implications in drug delivery vehicle design across nano-to-micro scale. Nanoscale 10, 15350–15364.
Del Monte, U., 2005. Swelling of hepatocytes injured by oxidative stress suggests pathological changes related to macromolecular crowding. Med. Hypotheses 64, 818–825.
Deng, Y., Zhang, Y., Lemos, B., Ren, H., 2017. Tissue accumulation of microplastics in mice and biomarker responses suggest widespread health risks of exposure. Sci. Rep. 7, 46687.
Deng, Y., ZhangY, Qiao, R., Bonilla, M.M., Yang, X., Ren, H., Lemos, B., 2018. Evidence that microplastics aggravate the toxicity of organophosphorus flame retardants in mice (Mus musculus). J. Hazard. Mater. 357, 348–354.
Ding, J., Zhang, S., Razanajatovo, R.M., Zou, H., Zhu, W., 2018. Accumulation, tissue distribution, and biochemical effects of polystyrene microplastics in the freshwater fish red tilapia (Oreochromis niloticus). Environ. Pollut. 238, 1–9.
Ellman, G.E., 1959. Tissue sulphydryl groups. Arch. Biochem Biophys. 82, 70–77.
Faddah, M.L., Abdel Baky, N.A., Al-Rasheed, N.M., Al-Rasheed, N.M., 2013. Biochemical responses of nanosize titanium dioxide in the heart of rats following administration of idepenone and quercetin. Afr. J. Pharm. Pharm. 7, 2639–2651.
Gelbke, H.P., BantonM, Block, C., Dawkins, G., Eisert, R., Leibold, E., Pemberton, M., Puijk, I.M., Sakoda, A., Yasukawa, A., 2019. Risk assessment for migration of styrene oligomers into food from polystyrene food containers. Food Chem. Toxicol. 124, 151–167.
Gigault, J., Halle, A.T., Baudrimont, M., Pascal, P.Y., Gauffre, F., Phi, T.L., El Hadri, H., Grassl, B., Reynaud, S., 2018. Current opinion: what is a nanoplastic? Environ. Pollut. 235, 1030–1034.
Han, B., Liu, W., Li, J., Wang, J., Zhao, D., Xu, R., Lin, Z., 2017. Catalytic hydrodechlorination of triclosan using a new class of anion-exchange-resin supported palladium catalysts. Water Res. 120, 199–210.
Hashim, A.R., Bashir, D.W., Yasin, N.A.E., Rashad, M.M., El-Gharbawy, S.M., 2022. Ameliorative effect of N-acetylcysteine on the testicular tissue of adult male albino rats after glyphosate-based herbicide exposure. J. Biochem. Mol. Toxicol., e22997 https://doi.org/10.1002/jbt.22997.
Hazeem, L.J., Yesilay, G., Bououdina, M., Perna, S., Cetind, D., Suludere, Z., Barras, A., Boukherroub, R., 2020. Investigation of the toxic effects of different polystyrene micro-and nanoplastics on microalgae Chlorella vulgaris by analysis of cell viability, pigment content, oxidative stress and ultrastructural changes. Mar. Pollut. Bull. 156, 111278.
Honary, S., Barabadi, H., Gharaei-Fathabad, E., Naghibi, F., 2012. Green synthesis of copper oxide nanoparticles using Penicillium aurantiogriseum, Penicillium citrinum and Penicillium waksmanii. Dig. J. Nanomater. Bios 7, 999–1005.
Hotti, A., Järvinen, K., Siivola, P., Hölttä, E., 2000. Caspases and mitochondria in c-Myc-induced apoptosis: identification of ATM as a new target of caspases. Oncogene 19, 2354–2362.
Hsu, S.M., Raine, L., Fanger, H., 1981. The use of antiavidin antibody and avidin-biotin-peroxidase complex in immunoperoxidase technics. Am. J. Clin. Pathol. 75 (6), 816–821.
Hu, M., Palić, D., 2020. Role of MicroRNAs in regulation of DNA damage in monocytes exposed to polystyrene and TiO2 nanoparticles. Toxicol. Rep. 7, 743–751.
Hu, Q., Wang, H., He, C., Jin, Y., Fu, Z., 2021. Polystyrene nanoparticles trigger the activation of p38 MAPK and apoptosis via inducing oxidative stress in zebrafish and macrophage cells. Environ. Pollut. 269, 116075.
Ibrahim, M.A., Khalaf, A.A., Galal, M.K., Ogaly, H.A., Hassan, A.H.M., 2015. Ameliorative influence of green tea extract on copper nanoparticle-induced hepatotoxicity in rats. Nanoscale Res. Lett. 10, 363.
Li, B., Ding, Y., Cheng, X., Sheng, D., Xu, Z., Rong, Q., Wu, Y., Zhao, H., Ji, X., Zhang, Y., 2020. Polyethylene microplastics affect the distribution of gut microbiota and inflammation development in mice. Chemosphere 244, 125492.
Livak, K.J., Schmittgen, T.D., 2001. Analysis of relative gene expression data using real-time quantitative PCR and the 2(-Delta Delta C (T)) method. Methods 25, 402–408.
Lu, L., Wan, Z., Luo, T., Fu, Z., Jin, Y., 2018. Polystyrene microplastics induce gut microbiota dysbiosis and hepatic lipid metabolism disorder in mice. Sci. Total Environ. 631, 449–458.
Luo, T., Wang, C., Pan, Z., Jin, C., Fu, Z., Jin, Y., 2019. Maternal polystyrene microplastic exposure during gestation and lactation altered metabolic homeostasis in the dams and their F1 and F2 offspring. Environ. Sci. Technol. 53, 10978–10992.
Manke, A., Wang, L., Rojanasakul, Y., 2013. Mechanisms of nanoparticle-induced oxidative stress and toxicity. Biomed. Res Int. 2013, 942916.
Méndez-García, L.A., Martínez-Castillo, M., Villegas-Sepúlveda, N., Orozco, L., Córdova, E.J., 2019. Curcumin induces p53-independent inactivation of Nrf2 during oxidative stress-induced apoptosis. Hum. Exp. Toxicol. 38, 951–961.
Michael, J.D., 2008. The Toxicologist's Pocket Handbook, 2nd ed.,. Informa Healthcare, New York, NY, USA.
Motaghinejad, M., Karimian, M., Motaghinejad, O., Shabab, B., Yazdani, I., Fatima, S., 2015. Protective effect of various dosage of Curcumin against morphine induced apoptosis and oxidative stress in rat isolated hippocampus. Pharm. Rep. 67, 230–235.
Neyrinck, A., 2004. Modulation of Kupffer cell activity: physio-pathological consequences on hepatic metabolism. Bull. Mem. Acad. R. Med. Belg. 159, 358–366.
Ohkawa, H., Ohishi, N., Yagi, K., 1979. Assay for lipid peroxides in animal tissues by thiobarbituric acid reaction. Anal. Biochem. 95, 351–358.
Oligny, L.L., Lough, J., 1992. Hepatic sinusoidal ectasia. Hum. Pathol. 23, 953–956.
Pitt, J.A., Trevisan, R., Massarsky, A., Kozal, J.S., Levin, E.D., Di Giulio, R.T., 2018. Maternal transfer of nanoplastics to offspring in zebrafish (Danio rerio): a case study with nanopolystyrene. Sci. Total Environ. 643, 324–334.
Qiao, R., Sheng, C., Lu, Y., Zhang, Y., Ren, H., Lemos, B., 2019. Microplastics induce intestinal inflammation, oxidative stress, and disorders of metabolome and microbiome in zebrafish. Sci. Total Environ. 662, 246–253.
Rashad, M.M., Galal, M.K., EL-BehairyAM, Gouda, E.M., Said, Z., Moussa, S.Z., 2018. Maternal exposure to di-n-butyl phthalate induces alterations of c-Myc gene, some apoptotic and growth-related genes in pups' testes. Toxicol. Ind. Health 34, 744–752.
Rhodes, C.J., 2018. Plastic pollution and potential solutions. Sci. Prog. 101, 207–260.
Roberts, R.A., Ganey, P.E., Ju, C., Kamendulis, L.M., Rusyn, I., Klaunig, J.E., 2007. Role of the Kupffer cell in mediating hepatic toxicity and carcinogenesis. Toxicol. Sci. 96, 2–15.
Rubio, L., Marcos, R., Hernández, A., 2020. Potential adverse health effects of ingested micro- and nanoplastics on humans. Lessons learned from in vivo and in vitro mammalian models. J. Toxicol. Environ. Health B Crit. Rev. 51–68.
Schrand, A.M., Rahman, M.F., Hussain, S.M., Schlager, J.J., David, A., Smith, D.A., Syed, A.F., 2010. Metal-based nanoparticles and their toxicity assessment. Nanomed. Nanobiotechnol. 544–568.
Semisch, A., Ohle, J., Witt, B., Hartwig, A., 2014. Cytotoxicity and genotoxicity of nano - and microparticulate copper oxide: role of solubility and intracellular bioavailability. Part Fibre Toxicol. 11, 10.
Sen, P., Xiong, Y., Zhang, Q., Park, S., You, W., Ade, H., Kudenov, M.W., O'Connor, B.T., 2018. Shear-enhanced transfer printing of conducting polymer thin films. ACS Appl. Mater. Interfaces 10, 31560–31567.
Smith, M., Love, D.C., Rochman, C.M., Neff, R.A., 2018. Microplastics in seafood and the implications for human health. Curr. Environ. Health Rep. 5 (3), 375–386.
Soenen, S.J., Parak, W.J., Rejman, J., Manshian, B., 2015. Intra) cellular stability of inorganic nanoparticles: effects on cytotoxicity, particle functionality, and biomedical applications. Chem. Rev. 115, 2109–2135.
Stock, V., Böhmert, L., Lisicki, E., Block, R., Cara-Carmona, J., Pack, L.K., Selb, R., Lichtenstein, D., Voss, L., Henderson, C.J., Zabinsky, E., 2019. Uptake and effects of orally ingested polystyrene microplastic particles in vitro and in vivo. Arch. Toxicol. 93 (7), 1817–1833.
Sun, C., Wang, Z.H., Liu, X.X., Yang, L.N., Wang, Y., Liu, Y., Mao, A.H., Liu, Y.Y., Zhou, X., Di, C.X., Gan, L., Zhang, H., 2015. Disturbance of redox status enhances radiosensitivity of hepatocellular carcinoma. Am. J. Cancer Res. 5, 1368–1381.
Tomasi, M.L., Ramani, K., 2018. Sumoylation and phosphorylation cross-talk in hepatocellular carcinoma. Transl. Gastroenterol. Hepatol. 3, 20.
Tonelli, C., Chio, I.I.C., Tuveson, D.A., 2018. Transcriptional regulation by Nrf2. Antioxid. Redox Signal 29, 1727–1745.
Wright, S.L., Kelly, F.J., 2017. Plastic and human health: a micro issue? Environ. Sci. Technol. 51, 6634–6647.
Xue, D., Zhou, X., Qiu, J., 2020. Emerging role of NRF2 in ROS-mediated tumor chemoresistance. Biomed. Pharm. 131, 110676.
Yang, Y.F., Chen, C.Y., Lu, T.H., Liao, C.M., 2019. Toxicity-based toxicokinetic/toxicodynamic assessment for bioaccumulation of polystyrene microplastics in mice. J. Hazard. Mater. 366, 703–713.
Yong, C.Q., Valiyaveetill, S., Tang, B.L., 2020. Toxicity of microplastics and nanoplastics in mammalian systems. Int. J. Environ. Res. Public Health 17, 1509.
Yu, Z., Li, Q., Wang, J., Yu, Y., Wang, Y., Zhou, Q., Li, P., 2020. Reactive oxygen species-related nanoparticle toxicity in the biomedical field. Nanoscale Res. Lett. 15, 115.
Zalasiewicz, J., Waters, C.N., Ivar do Sul, J.A., Corcoran, P.L., Barnosky, A.D., Cearreta, A., Edgeworth, M., Gałuszkah, A., Jeandel, C., Leinfelder, R., McNeill, J.R., Steffen, W., Summerhayes, C., Wagreich, M., Williams, M., Wolfe, A.P., Yonan, Y., 2016. The geological cycle of plastics and their use as a stratigraphic indicator of the Anthropocene. Anthropocene 13, 4–17.
Zhao, M., Su, J., Head, E., Cotman, C.W., 2003. Accumulation of caspase cleaved amyloid precursor protein represents an early neurodegenerative event in aging and in Alzheimer's disease. Neurobiol. Dis. 14, 391–403.
Zheng, L., Cai, G., Wang, S., Liao, M., Li, Y., Lin, J., 2019. A microfluidic colorimetric biosensor for rapid detection of Escherichia coli O157: H7 using gold nanoparticle aggregation and smart phone imaging. Biosens. Bioelectron. 124, 143–149.
Zuccarello, P., Ferrante, M., Cristaldi, A., Copat, C., Grasso, A., Sangregorio, D., Fiore, M., Conti, G.O., 2019. Exposure to microplastics (< 10 μm) associated to plastic bottles mineral water consumption: the first quantitative study. Water Res. 157, 365–371.